OLGA DOCENKO

HIGH-RESOLUTION SPECTROSCOPY OF THE GROUND AND SELECTED EXCITED STATES OF THE NaRb AND NaCs MOLECULES

Summary of the Thesis

Scientific supervisors:
Leading researcher, Dr. habil phys. Māris Tamanis
Professor, Dr. habil phys. Ruvins Ferbers

University of Latvia

Riga – 2006

Abstract

Thesis is devoted to high resolution spectroscopic studies of heteronuclear alkali dimers. Research objects are NaRb and NaCs molecules. They were chosen to respond the demand for accurate spectroscopic information on the electronic states of these molecules, especially the ground states, due to growing interest to cold collision experiments with Na–Rb and Na–Cs pairs. Besides, the theoretical calculations needed a comparison with reliable experimental data. Therefore the following main goal of the present research was introduced: to obtain accurate spectroscopic information on the ground and selected excited states of the NaRb and NaCs molecules. The method applied is a Fourier transform spectroscopy of Laser induced fluorescence. For the first time the $X^1\Sigma^+$, $a^3\Sigma^+$, $C^1\Sigma^+$, $D^1\Pi$ states of NaRb and $X^1\Sigma^+$, $a^3\Sigma^+$ states of NaCs have been studied experimentally with high accuracy in a wide range of internuclear distances. Accurate empirical potential energy curves of these states have been determined and compared with the recent theoretical calculations. Our work has demonstrated that Fourier transform spectroscopy of laser induced florescence is a powerful tool for studying not only of ground states, but also excited states due to collision induced transitions. The results obtained in the course of work open path for new experimental studies, e.g. dynamic and structural studies of these molecules and cold collision experiments with atomic pairs.
Thesis consists of Abstract, 6 Chapters, including Introduction and Conclusions (105 pages, 50 figures and 18 Tables), and of References (105 citations). Thesis is written in the English language.

Introduction

Motivation

Alkali-metal diatomic molecules have been a subject of scientific research for already more than a century since the first observation of Na_2 fluorescence in 1891 [1]. A lot of significant results have been obtained in this field already in pre-laser epoch [2, 3], but a real breakthrough has happened after invention of a laser. And since then alkali-metal diatomic molecules have proved to be in a focus of intensive experimental and theoretical studies. This is explained by the fact that they are the simplest molecules consisting from atoms having only one valence electron, therefore they can be used as test objects to probe different theoretical approaches. Understanding the structure of diatomic molecules is an essential step from atoms to bigger molecules. From the experimental point of view these molecules can be produced relatively easy and their spectra can be excited with variety of conventional laser sources (Ar^+, He–Ne, dye lasers, etc.). From these experiments researchers can derive information about potential energy curves (PEC) of molecular states, permanent electric dipole moments, lifetimes, transition dipole moments, etc. and compare them with theoretical calculations. In spite of seemingly simple structure of alkali-metal dimers accuracy of fully theoretical (*ab initio*) calculations is not yet sufficient, due to the fact that Schrödinger equation cannot be solved analytically for these molecules, and approximations are used. For example, discrepancy of empirical and theoretical potential energy curves for heteronuclear dimers can reach several hundreds cm^{-1}, versus experimental error of less than 0.1 cm^{-1}. Therefore comparison with experimental data is essential for making choice among different models and theoretical approaches.

Homonuclear alkali dimers (e.g. Na_2, K_2) are the best studied diatomic alkali molecules. There is much less information on heteronuclear alkali molecules. The best studied heteronuclear alkali dimer is NaK molecule. There are still large gaps in knowledge of the structure of other molecules and the task of the molecular spectroscopy is to obtain accurate information about different electronic states, especially the ground state. Experimental knowledge of the ground state is essential, as all molecular transitions have their origin there. Accurate description of the ground state in the form of molecular constants or PEC is demanded for assignment of observed transitions, which is, in turn, a necessary step for further studies of excited states. Also knowledge of ground state PEC allows one to construct the so-called difference-based potentials from the *ab initio* PECs [4]. In a number of cases this approach yields a much better representation of excited molecular states compared to pure *ab initio*. Study of diatomic molecules also provides information about interactions of electronic states through observations of perturbations in the spectra [5]. For example, study of phenomena like Λ-doubling allows one to measure directly the strength of intramolecular $^1\Pi \sim {}^1\Sigma^{\pm}$ interaction, yielding an essentially novel insight into the structure not only of an isolated $^1\Pi$ state, but of a $^1\Pi \sim {}^1\Sigma^{\pm}$ complex.

Especial interest is put on studies of the ground and lowest triplet states near the asymptote. This is motivated by the other field of research of alkali dimers—formation of cold molecules. Currently, the goal of many researchers in the fields of atomic and molecular physics, physical chemistry and chemical physics is to produce dense samples of ultracold[1] polar molecules (see Special issue on Cold Molecules [6] and references therein). This interest is motivated by the fact that molecules offer intriguing properties which are not available with atoms. This especially applies to heteronuclear molecules, which have permanent electric dipole moments. Formation of ultracold molecules is of actual interest for such fields as: controlling chemical reactions and collisions (ultracold chemistry) [7]; observation of Bose-Einstein condensation (BEC) and Fermi degeneracy with molecules; high resolution molecular spectroscopy; tests of fundamental theories such as search for an electric dipole moment of the electron [8, 9]; quantum computation using aligned molecular dipoles as qubits [10], etc. The development of cold molecule formation schemes appears to be crucially dependent on *accurate spectroscopic information* about the molecules and on *active interplay between theory and experiment* (see Ref. [11, 12] and references therein).

Heteronuclear diatomic molecules are also interesting objects for applied science. For example, prospective application of polar diatomics, especially in the $^1\Pi$ states, is connected with their usage

[1] As "cold" usually designate molecules with translational temperatures between 1 and 1000 mK, and as "ultracold"—with translational temperature less than 1 mK.

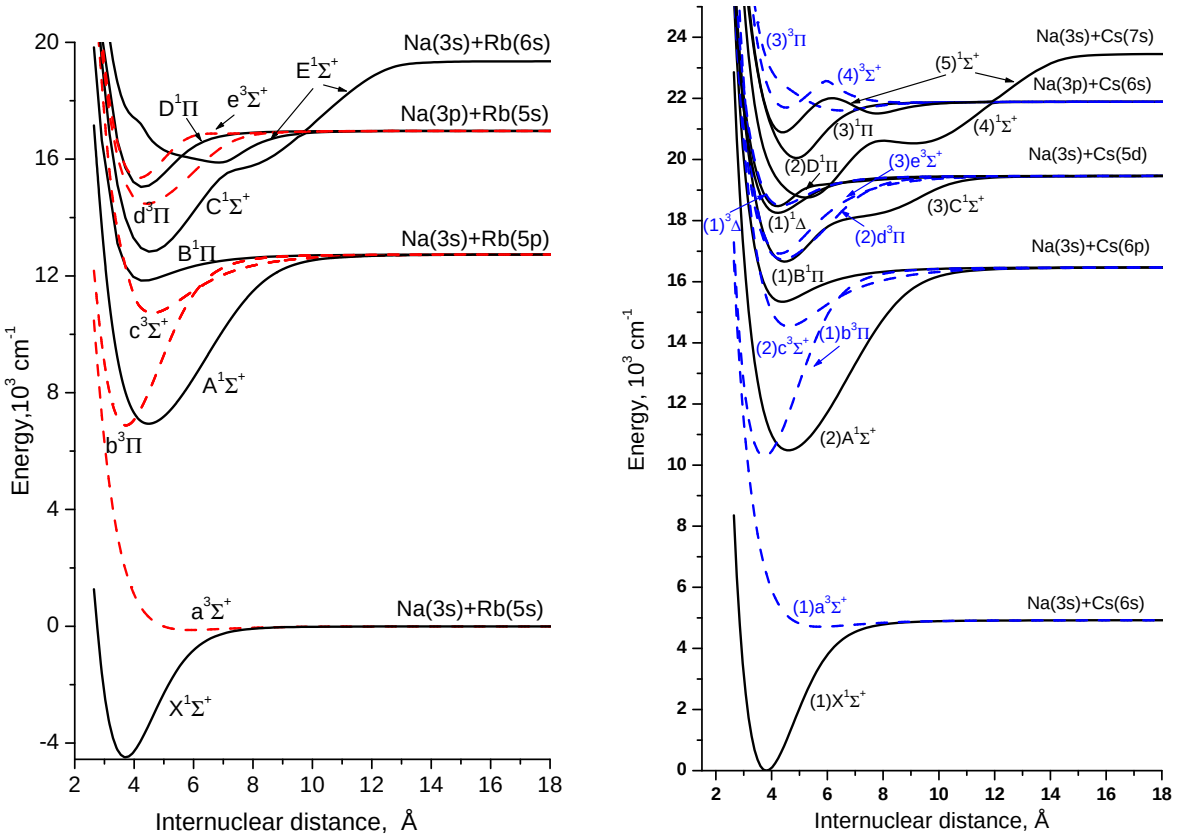

Figure 1. Potential energy curves for the low lying singlet and triplet states of NaRb [18] and NaCs [19] from *ab initio* calculations.

for sensitive non-contact probing and mapping of external electric field distribution via changes in laser-induced fluorescence caused by parity mixing due to quasi-linear Stark effect [13, 14].

Research objects and goals

Research objects of the present Thesis are **NaRb** and **NaCs** molecules. They were chosen to respond the demand for accurate spectroscopic information on the electronic states of these molecules, especially the ground states, due to growing interest to cold collision experiments with Na–Rb [15, 16] and Na–Cs [17] pairs. Besides, the *ab initio* calculations [18, 19, 4] needed a comparison with reliable experimental data. Therefore the following main **goals** of the present research were introduced:

1. To obtain the NaRb $X^1\Sigma^+$ and $a^3\Sigma^+$ state accurate empirical PECs in a wide range of internuclear distances and to perform the combined analysis of these states taking into account hyperfine mixing.
2. To obtain the NaRb $C^1\Sigma^+$ state accurate empirical PEC.
3. To obtain the NaRb $D^1\Pi$ state accurate empirical PEC, to study Λ-splitting in this state.
4. To obtain the NaCs $X^1\Sigma^+$ and $a^3\Sigma^+$ state accurate empirical PECs in a wide range of internuclear distances; to perform the combined analysis of these states taking into account hyperfine mixing.

Method and tasks

The **method** chosen for fulfilling these goals is a *Laser Induced Fluorescence* (LIF) method. The following methodological **tasks** have been formulated:

1. To prepare experimental setup for performing LIF measurements in the NaRb and NaCs molecules.
2. To excite electronic transitions in NaRb and NaCs, involving the states of interest, by using different laser sources.
3. To perform vibrational, rotational and isotopomer assignment of progressions in electronic spectra, as well as for rotational relaxation transitions. In the case of the $D^1\Pi$ state to analyse the derived Λ-splittings.
4. To perform a fitting procedure of potential energy curves to experimental data. To analyse the quality of potentials and to compare with available *ab initio* data.

A number of experiments have been carried out in order to realize these tasks. The initial part of experiments (NaRb $X^1\Sigma^+$ state) was done in Riga, in the Laboratory of Optical Polarization of Molecules (head Prof. R. Ferber), Institute of Atomic Physics and Spectroscopy, University of Latvia. The further experiments were performed using high-resolution Fourier-transform spectrometer in the laboratory of Prof. E. Tiemann, Institute of Quantum Optics, University of Hannover.

The structure of the Thesis is the following. In the Second Chapter the theoretical background of the performed research is briefly given. In the Third Chapter the experimental setups are described. In the Fourth Chapter the results on the NaRb $X^1\Sigma^+$, $a^3\Sigma^+$, $C^1\Sigma^+$ and $D^1\Pi$ states are presented, whereas the Fifth Chapter is devoted to the NaCs $X^1\Sigma^+$ and $a^3\Sigma^+$ states. Results and conclusions are given in Chapter 6.

Publications

The main results of the Thesis are presented in the following scientific papers:

[dis1] **O. Docenko**, O. Nikolayeva, M. Tamanis, R. Ferber, E.A. Pazyuk and A.V. Stolyarov, *Experimental studies of the NaRb ground state potential up to* $v'' = 76$ *level*, Physical Review A 66, 052508 (2002).

[dis2] **O. Docenko**, M. Tamanis, R. Ferber, A. Pashov, H. Knöckel, and E. Tiemann, *Potential of the ground state of NaRb*, Physical Review A 69, 042503 (2004).

[dis3] A. Pashov, **O. Docenko**, M. Tamanis, R. Ferber, H. Knöckel, E. Tiemann, *Potentials for modeling cold collisions between Na (3S) and Rb (5S) atoms*, Physical Review A 72, 062505 (2005).

[dis4] W. Jastrzebski, P. Kortyka, P. Kowalczyk, **O. Docenko**, M. Tamanis, R. Ferber, A. Pashov, H. Knöckel, E. Tiemann, *Accurate characterisation of the* $C(3)^1\Sigma^+$ *state of the NaRb molecule*, European Physical Journal D 36, 57-65 (2005).

[dis5] **O. Docenko**, M. Tamanis, R. Ferber, A. Pashov, H. Knöckel, E. Tiemann, *The* $D^1\Pi$ *state of the NaRb molecule*, European Physical Journal D 36, 49-55 (2005).

[dis6] **O. Docenko**, M. Tamanis, R. Ferber, A. Pashov, H. Knöckel, E. Tiemann, *Spectroscopic studies of NaCs for the ground state asymptote of Na + Cs pairs*, European Physical Journal D 31, 205-211 (2004).

The obtained results have been reported in a number of international conferences, which is reflected in the following conference abstracts:

- **O. Docenko**, I. Klincare, O. Nikolayeva, M. Tamanis, R. Ferber, E.A. Pazyuk and A.V. Stolyarov, *Laser induced fluorescence studies of the NaRb molecule ground state up to* $v'' = 76$, in Abstracts of the 34th EGAS Conference (Sofia, Bulgaria, July 9-12, 2002), 26C, p. 80-81.
- **O. Docenko**, I. Klincare, O. Nikolayeva, M. Tamanis, R. Ferber, E. A. Pazyuk and A. V. Stolyarov, *Spectroscopic studies of the NaRb ground state up to near - dissociation limit*, , in Abstracts of the 17th International Conference on High Resolution Spectroscopy (Prague, Czech Republic, September 1-5, 2002) p. 185.
- **O. Docenko**, M. Tamanis, R. Ferber, A. Pashov, H. Knöckel, E. Tiemann, *Fourier-transform spectroscopy of NaRb*, 35th EGAS conference, in Abstracts of the 35th EGAS Conference (Brussels, Belgium, July 15-18, 2003), 27B, p. 65.
- **O. Docenko**, M. Tamanis, R. Ferber, A. Pashov, H. Knöckel, E. Tiemann, *Fourier-transform spectroscopy studies of the NaRb molecule*, in Abstracts of the workshop Non-destructive electric field imaging and high-frequency plasma applications for nanoscale surface treatment (Riga, August 21-22, 2003), p.10.
- **O. Docenko**, M. Tamanis, R. Ferber, A. Pashov, H. Knöckel, and E. Tiemann, *The* $D^1\Pi$ *state of the NaRb molecule*, in Abstracts of the ECAMP 8 conference (Rennes, France, July 6-10, 2004), 28F, vol. 2, p. 43.
- **O. Docenko**, M. Tamanis, R. Ferber, A.Pashov, H. Knöckel, and E. Tiemann, *The* $a^3\Sigma^+$ *state of the NaRb molecule*, in Abstracts of the ECAMP 8 conference, 28F, vol. 2, p. 44.
- **O. Docenko**, M. Tamanis, R. Ferber, A. Pashov, H. Knöckel, and E. Tiemann, *The ground state of NaCs*, in Abstracts of the ECAMP 8 conference, 28F, vol. 2, p. 45.
- W. Jastrzebski, P. Kortyka, P. Kowalczyk, **O. Docenko**, M. Tamanis, R. Ferber, A. Pashov, H. Knöckel, and E. Tiemann, *The accurate* $C^1\Sigma^+$ *state potential of the NaRb molecule*, in Abstracts of the ECAMP 8 conference, 28F, vol. 2, p. 85.
- H. Knöckel, **O. Docenko**, E. Zaharova, M. Tamanis, R. Ferber, A. Pashov, and E. Tiemann, *Spectroscopic studies of the NaCs triplet ground state*, in Verhandlungen der Deutschen Physikalischen Gesellschaft (Berlin, March 4-9, 2005), p. 70.
- **O. Docenko**, J. Zaharova, M. Tamanis, R. Ferber, A. Pashov, H. Knöckel, E. Tiemann, The $a^3\Sigma^+$ state of the NaCs molecule, in Abstracts of the 37th EGAS Conference (Dublin, Ireland, August 3-6, 2005), 29I, p. 189.

Experimental setup

The Third Chapter is devoted to the description of the experimental setups. Chapter is divided into two parts corresponding to the experiments performed at the University of Latvia and University of Hannover.

In the experiments performed at the University of Latvia LIF was excited by an Ar^+ laser (Spectra Physics 171) operating in a single-mode regime at 514.5 nm wavelength. LIF has been dispersed by a double monochromator DFS-12 with 1200 lines/mm gratings and 5 Å/mm inverse dispersion in the first diffraction order, providing at reasonable slits 0.2 Å spectral resolution. Fluorescence progressions have been detected up to 680 nm by a FEU-79 photomultiplier operating in a photon counting regime. Simultaneously detected Ar and Ne discharge lines have been used as frequency standards. The average uncertainty of LIF line positions was estimated as ca. 0.1 cm^{-1}. NaRb molecules were formed from a 4:1 mixture (by weight) of natural Rb (containing 72% of ^{85}Rb and 28% of ^{87}Rb) and Na metals in an alkali-resistant glass thermal cell at temperature ca. 550 K. The cell was heated in a two part resistance

oven, maintaining app. 20 K higher temperature of the upper part than the lower one in order to prevent metal condensation in the upper part of the glass cell.

In the experiments in Hannover for preparation of the molecules a heat-pipe oven or a metal cell were used. A single section heat-pipe cell is made of a stainless steel tube. The inner part of the heat-pipe is covered by a fine metal mesh. Each end of the tube is closed by a glass window with antireflection coating. The end parts are water cooled. In order to prevent atom condensation on the windows, the buffer gas is used. As buffer gas we used argon with typical pressure of few millibars (mbar).

NaRb molecules were produced in a heat-pipe oven by heating 5 g of Na and 10 g of Rb (natural isotopic composition) from Alfa Aesar. The oven was operated at temperatures between 560 K and 600 K and typically with 2 mbar of Ar as buffer gas.

For experiments with NaCs in order to ensure safe operation with Cs, a metal cell was designed. The advantages of using the metal cell compared to the traditional heat-pipe ovens are the safe procedures for loading, the possibility for operation with small amounts of metals, and also without presence of buffer gas. Usually the cell was heated to 550–600 K and operated without buffer gas. Unfortunately, after about 20 hours of operation a leak in the sapphire windows of the cell was found. For longer experimental studies a heat-pipe oven was designed as described above which was provided with a short metal container welded to the central part of the pipe for safe Cs load. 5 g Cs and ca. 10 g of Na were used. The oven was operated at temperatures between 560 K and 600 K and typically with 3 mbar of Ar as a buffer gas.

Several different types of cw lasers were used in the present experiments.

1. Ar^+ laser (Spectra Physics BeamLok 2060) operated at lines 514.5, 501.7, 496.5, 488.0, 476.5 nm in a multimode (typical power 0.5-3 W) and a single mode regime (typical power 100-500 mW).

2. Tuneable single-mode frequency doubled Nd:YAG laser with a typical output power of 70 mW at 532.2 nm. Tuning range app. 3 cm^{-1}.

3. Ring dye laser Coherent 699-21 with Rhodamine 6G dye (tuning range 550–590 nm, peak at 560 nm) with power ca. 100 mW, pumped by Nd:YAG frequency doubled laser (Verdi, Coherent).

4. Linear dye laser Coherent 599 with DCM dye (tuning range 610–695 nm, peak at 645 nm) with power ca. 70 mW, pumped by Ar^+ laser.

LIF was analysed with the help of the Fourier Transform Spectrometer IFS 120 from Bruker Optics. It operates (with appropriate change of optics and detectors) in a spectral range from 63200 cm^{-1} in the ultraviolet region to 450 cm^{-1} in the infrared region. The instrument allows to obtain relative accuracy better than $0.5 \cdot 10^{-7}\sigma$ and an absolute accuracy better than $5 \cdot 10^{-7}\sigma$, where σ is a frequency in wavenumbers. In the region of 20000 cm^{-1} it corresponds to 0.001 cm^{-1} and 0.01 cm^{-1} accuracies, respectively.

The LIF signal was detected with a Hamamatsu R928 photomultiplier tube or a silicon diode depending on the desired wavelength region. The scanning path of the spectrometer was set to reach a typical resolution of 0.0115 cm^{-1}– 0.03 cm^{-1} and the typical number of scans for averaging varied between 10 and 20. In order to avoid the illumination of the detector by the He-Ne laser, used for calibration of the spectrometer, a NOTCH interference filter with 8 nm full width at half maximum was introduced. For better signal-to-noise ratio some spectra were recorded by limiting the desired spectral window with colored glass or interference filters.

NaRb molecule

The Fourth Chapter is devoted to the studies of the NaRb molecule. **The First Subchapter** contains a review of literature data on this molecule. Summarising, at the moment of the beginning of this work most of information on the NaRb electronic states was fragmentary and of accuracy, insufficient for demands of modern spectroscopy, especially cold collision physics. Available information on the $X^1\Sigma^+$ state was of high accuracy, but limited at $v'' = 30$ and low J'' [20]. The lowest triplet $a^3\Sigma^+$ state was

studied in a wide range, but with low accuracy [21]. $D^1\Pi$ state was also investigated in a limited range of quantum numbers with low accuracy [4]. $C^1\Sigma^+$ state has never been observed previously.

NaRb $X^1\Sigma^+$ state: Experiments at the University of Latvia

The Second Subchapter is devoted to the studies of the $X^1\Sigma^+$ state performed at the University of Latvia [dis1]. During the studies on the permanent electric dipole moments and q factors in the $B^1\Pi$ and $D^1\Pi$ states of NaRb performed at the University of Latvia [22, 4] it was realized that information on the $X^1\Sigma^+$ ground state is insufficient, therefore we put forward a **goal** to obtain accurate $X^1\Sigma^+$ state potential, which would be applicable in a wide range of vibrational and rotational quantum numbers.

The usual way of extending the range of ground state vibrational levels v'' observed in emission for alkali dimers is to use, instead of the B–X, either the A–X or C–X system. In the present study we made use of the opportunity to excite the high vibrational levels of the $C^1\Sigma^+$ electronic state in a direct $C^1\Sigma^+ \leftarrow X^1\Sigma^+$ transition and to exploit the subsequent visible emission. In our experiments we used the Ar^+ 514.5 nm line for exciting the $C^1\Sigma^+ \rightarrow X^1\Sigma^+$ progressions, which stem up to $v'' = 76$ thus providing us data about vibrational levels $v'' > 30$. We have registered and assigned five $C^1\Sigma^+ \rightarrow X^1\Sigma^+$ fluorescence progressions.

The total data set included in the analysis of the $X^1\Sigma^+$ state term values was constructed of three parts. The first part contains the present measured 302 term values assigned to both $Na^{85}Rb$ and $Na^{87}Rb$ isotopomers corresponding to $v'' \in [24, 76]$; $J'' \in [12, 64]$ levels. The second part contains 44 highly accurate (with a line position uncertainty 0.003 cm^{-1}) experimental term values for $v'' \in [5, 30]$; $J'' = 10, 12$ levels of $Na^{85}Rb$ given in Ref. [20]. The third part contains eight $v'' \in [0, 3]$; $J'' = 10, 12$ term values restored using the relevant G_v, B_v, D_v and H_v molecular constants of the $Na^{85}Rb$ isotopomer given in Ref. [21] with uncertainty of 0.003 cm^{-1}.

Term values for the isotope-substituted NaRb molecule were represented by a Dunham expansion. The resulting $G(v'')$ and $B(v'')$ expansions were further applied to a conventional RKR potential construction up to the last observed vibrational level $v'' = 76$. A non-physical bend (a "turning over") had appeared in the inner wall of the RKR curve for $v'' \geq 55$ levels. This means that the obtained vibrational and rotational constants are not self-consistent for upper vibrational levels due to strong correlation between the rotational and centrifugal distortion constants. The bend problem was solved by the exponential extrapolation of the inner wall and respective correction of the outer wall. To consistently process different sets of experimental and theoretical data, we applied a direct potential fit analysis based on the Morse-Lennard-Jones (MLJ) potential, which was proposed in Ref. [23]

$$U_{MLJ}(R) = D_e \left[1 - \left(\frac{R_e}{R}\right)^n \exp\left[-\beta_{MLJ}(z)z\right]\right]^2 . \quad (1)$$

The power $n = 6$ predicts correct long-range behavior of the NaRb ground state potential $U(R) \sim D_e - C_6/R^6$ dissociated into two ^1S state atoms. In the z-region covered by the experimental term values the exponent parameter $\beta(z)$ is approximated by the ordinary polynomial expansion $\sum_{m=0}^{M} \beta_m z^m$. The dispersion coefficient C_6 was taken from Ref. [24]. The matching point $R_M = 11$ Å was fixed at near the right turning point of the last observed vibrational level $v'' = 76$. The equilibrium distance R_e, polynomial coefficients β_m ($m \in [0, 9]$), as well as the origins of the present five LIF series were considered as adjustable fitting parameters during the weighted non-linear least-squares fit. The resulting MLJ potential reproduces low J term values from Refs. [20, 21] with r.m.s.= 0.004 cm^{-1} while the present experimental term values with r.m.s.= 0.1 cm^{-1}.

Results and conclusions

1. LIF spectra to the NaRb $X^1\Sigma^+$ ground state up to $v'' = 76$ were recorded for the first time using $C^1\Sigma^+ \rightarrow X^1\Sigma^+$ transitions. The obtained data set consists of 300 transitions in $Na^{85}Rb$ and $Na^{87}Rb$ to ground state levels in the range $v'' = 24 - 76$, $J'' = 12 - 64$, with typical accuracy of 0.1 cm^{-1}. The last observed level is ($v'' = 76$, $J'' = 27$).

2. Transition frequencies were used for a direct fit of a MLJ potential energy curve. The fitted potential describes the present experimental data with r.m.s.= 0.1 cm^{-1}. Experimental PEC covers 99.85% of the potential well depth. Term energies were also represented by the Dunham expansion and RKR potential.

3. MLJ construction allowed us to match gently the previous highly accurate experimental term values available for the bottom of the potential with its long-range behavior through the intermediate v'' region completely covered by the present measurements. In spite of the moderate accuracy of the current measurements (0.1 cm^{-1}) the derived MLJ potential significantly improves the description of the NaRb $X^1\Sigma^+$ ground state in the $v'' \gtrsim 35$ region.

4. Highly accurate experimental term values for the extended range of rotational levels would be desirable for further improvement of the ground state potential.

5. $C^1\Sigma^+$ state has been observed for the first time. Rotational and isotopomer assignment of five levels has been made.

NaRb $X^1\Sigma^+$ state: Experiments at the University of Hannover

The Third Subchapter is devoted to the studies of the $X^1\Sigma^+$ state performed at the University of Hannover. In the experiments in Hannover the NaRb molecules were studied with the same LIF method but two important changes compared to the Riga experiments have been introduced: producing of molecules in a heat pipe oven and fluorescence analysis with Fourier transform spectrometer. Also a great advantage of the laboratory in Hannover is a variety of available laser sources.

The Ar^+ laser 514.5 nm, 501.7 nm, 496.5 nm, 488.0 nm, and 476.5 nm lines induced fluorescence mainly due to the $D^1\Pi \rightarrow X^1\Sigma^+$ transitions in NaRb. Along with the D←X system, the 514.5 nm line excites also transitions in the $C^1\Sigma^+ \leftarrow X^1\Sigma^+$ system of NaRb, as was established in our experiments in Riga [dis1]. Ar^+ laser line 501.7 nm also excites the C state, but the resulting fluorescence is very weak. Only one progression was identified. The Nd:YAG laser excited the $C^1\Sigma^+ \leftarrow X^1\Sigma^+$ and $D^1\Pi \leftarrow X^1\Sigma^+$ systems of NaRb. The frequency was varied between 18787.25 cm^{-1} and 18788.44 cm^{-1}. The Rhodamine 6G laser excites the $B^1\Pi \leftarrow X^1\Sigma^+$ transitions and also weak transitions in the $C^1\Sigma^+ \leftarrow X^1\Sigma^+$ system and was used for two reasons. The first was to enrich the information on the ground-state levels and second, we wanted to excite levels of the $B^1\Pi$ state with significant triplet admixture due to perturbations from the neighboring $c^3\Sigma^+$ and $b^3\Pi$ states [21, 25]. Indeed, scanning the frequency of the dye laser from 16729 cm^{-1} to 16965 cm^{-1} we encountered a large number of excitations where a second fluorescence band around 12000 cm^{-1} appeared along with the B←X system. The analysis of this band confirmed that we have observed transitions to the $a^3\Sigma^+$ state .

The assignment of the recorded spectra was simplified by the MLJ potential obtained from the experiments performed in Riga. First, spectra induced by the Ar^+ laser were assigned, because they were partly known from the low-resolution studies [26, 22, 4, dis1]. Identification of 5 C→X progressions from previous studies was clearly confirmed by high-resolution measurements. Identification procedure was much faster that in the case of monochromator data due to high precision of the FTS data. The total data set consists of more than 6150 transitions in $Na^{85}Rb$ and 2650 in $Na^{87}Rb$.

The ground singlet states of both isotopomers of NaRb are described in the adiabatic approximation with a single potential-energy curve. The potential was constructed with an inverted perturbation approach (IPA) method as a set of points $\{R_i, U(R_i)\}$ connected with cubic spline function [27]. In order to exclude any fitting parameters concerning the excited states, we fitted the ground-state potential directly to the observed differences between ground-state levels [28]. The typical relative line uncertainty is 0.003 cm^{-1}. For $R > R_{out}$ we adopted the usual dispersion form

$$U(R) = D_e - \frac{C_6}{R^6} - \frac{C_8}{R^8} - \frac{C_{10}}{R^{10}} \qquad (2)$$

with coefficients C_6, C_8 taken from Refs. [29, 30]. The connecting point R_{out} and the parameters D_e and C_{10} were varied in order to ensure a smooth connection with the pointwise potential. The final set of potential parameters consists of 51 points.

Results and conclusions

1. High-resolution LIF spectra to the NaRb $X^1\Sigma^+$ ground state were obtained for the first time using the FTS method. The obtained data set consists of more than 6150 transitions in $Na^{85}Rb$ and 2650 in $Na^{87}Rb$ to the ground state levels in the range $J'' = 1 - 200$, $v'' = 0 - 76$, with typical uncertainty of 0.003 cm^{-1}.

2. Transition frequencies were used for a direct fit of a spline-pointwise potential energy curve. The fitted potential describes more than 43300 differences between 4090 energy levels of both isotopomers with a standard deviation σ=0.0031 cm^{-1} and a normalized standard deviation of $\bar{\sigma}$=0.70.

3. Experimental PEC covers 99.85% of the potential well depth. The classical turning point of the last observed energy level ($v'' = 76$, $J'' = 27$) is around 12.4 Å and this level is about 4.5 cm^{-1} below the asymptote.

4. Term energies were also fitted to the Dunham expansion. Obtained set of constants reproduces the experimental term energies with $\sigma = 0.003$ cm^{-1} and $\bar{\sigma} = 0.84$.

Combined analysis of the NaRb $a^3\Sigma^+$ and $X^1\Sigma^+$ states

The Fourth Subchapter is devoted to the studies of the $a^3\Sigma^+$ state and combined analysis of the NaRb $a^3\Sigma^+$ and $X^1\Sigma^+$ states [dis3]. The experimental data on the lowest triplet state $a^3\Sigma^+$ of NaRb until now were scarce [20] or obtained at low resolution [21]. **The goal** of the present experiments was twofold: extending experimental information about the triplet $a^3\Sigma^+$ state and collecting data close to the NaRb ground state asymptote, see Fig. 1a. This would allow us to derive more reliable $X^1\Sigma^+$ and $a^3\Sigma^+$ state potentials at large internuclear distances. Constructing the appropriate Hamiltonian for the problem, it should be taken into account that both states, $a^3\Sigma^+$ and $X^1\Sigma^+$, couple by hyperfine interaction, which for the most weakly bound states is of the same order of magnitude as the binding energy itself. Thus close to the asymptote these states loose their triplet or singlet character and coupled channels treatment should be applied.

A well known technique for reaching the triplet manifold from singlet states is through singlet and triplet molecular states mixed by perturbations (e.g. the spin-orbit coupling). Such perturbations between the $B^1\Pi$, $b^3\Pi$ and $c^3\Sigma^+$ states were reported by Wang *et al.* [21, 25]. Therefore, we used a Rhodamine 6G single mode dye laser and excited transitions to levels of the $B^1\Pi$, $b^3\Pi$ and $c^3\Sigma^+$ complex.

Assignment of the observed spectra was made using the $a^3\Sigma^+$ state hybrid potential from Ref. [31], based on the experimental data by Katô group [21]. Assignment was also checked, where it was possible, by finding the corresponding $B^1\Pi \rightarrow X^1\Sigma^+$ transition or checking laser resonance in B-X transition. Distinguishing between different isotopomers was simplified by the HFS of the triplet lines, which was partially resolved.

In order to observe transitions to weakly bound singlet and triplet ground state levels close to the atomic asymptote from a common upper level we took advantage of the long range changeover, namely that close to the atomic asymptote the Hund's case (a) and (b) electronic states develop to the Hund's case (c) coupling and finally to the Hund's case (e) where the electronic angular momenta are uncoupled from the molecular axis. That is, the $c^3\Sigma^+$ state at long internuclear distances becomes a mixed state with triplet and singlet character giving rise to transitions to the ground $a^3\Sigma^+$ and $X^1\Sigma^+$ states. In our experiments we observed several spectra which we interpret by such long-range changeover. This allowed us to collect abundant information on the near asymptotic levels of the $a^3\Sigma^+$ and $X^1\Sigma^+$ states.

The total data set for the $a^3\Sigma^+$ state consists of more than 900 transition frequencies to 490 energy levels for both isotopomers $Na^{85}Rb$ and $Na^{87}Rb$. The typical experimental uncertainty is 0.003 cm^{-1}.

The data set for the $X^1\Sigma^+$ state obtained previously, see [dis2] was correspondingly enriched by about 250 transitions adding some 150 new rovibrational levels.

The hyperfine structure free positions of the triplet state levels are shifted from the central component of the hyperfine pattern by 0.017 cm^{-1} for $Na^{85}Rb$ and by 0.062 cm^{-1} for $Na^{87}Rb$. By using these energy levels, potentials without HFS corrections were obtained.

At the first stage of the analysis we applied a single-potential approach for describing the experimental observations of the $a^3\Sigma^+$ state. The levels corrected for hyperfine structure were used to construct a potential curve for the $a^3\Sigma^+$ state in a manner similar to that used for the $X^1\Sigma^+$ state. Using the isotopic effect we revised the vibrational numbering of the $a^3\Sigma^+$ state (v was increased by 1) established for the first time in Ref. [20].

The final forms of the $X^1\Sigma^+$ and $a^3\Sigma^+$ state potentials were determined in a coupled channels analysis which takes into account the hyperfine interaction between these states. For large internuclear distances (typically larger than 11 Å) we adopted the standard long range form of molecular potentials:

$$U_{\rm LR}(R) = D - \frac{C_6}{R^6} - \frac{C_8}{R^8} - \frac{C_{10}}{R^{10}} \pm E_{ex}, \tag{3}$$

where the exchange contribution is given by

$$E_{ex} = A_{ex} R^{\gamma} \exp(-\beta R). \tag{4}$$

Here D is the energy of the atomic asymptote with respect to the minimum of the $X^1\Sigma^+$ state. It coincides with the dissociation energy of this state, $D_e^{\rm X}$. The exchange energy is repulsive for the triplet state (plus sign in (3)) and attractive for the singlet state (minus sign). All parameters in Eqs. (3,4) are common for the $X^1\Sigma^+$ and $a^3\Sigma^+$ states.

Since the analysis of the molecular hyperfine structure has shown that the corresponding splitting is independent of the vibrational and rotational structure and on average agrees with the atomic values, the interactions that couple the $X^1\Sigma^+ - a^3\Sigma^+$ system can be modeled by the atomic hyperfine splitting of the corresponding atoms. The total Hamiltonian describing the interactions between ground state Na and Rb atoms contains the kinetic energy operator for the relative radial motion between two atoms, the Born-Oppenheimer potentials for the $X^1\Sigma^+$ and $a^3\Sigma^+$ states, a hyperfine contact interaction for Na atom and Rb atom, and the nuclear rotation. Weak magnetic spin-spin and second-order spin-orbit interactions can be neglected for the purpose of this study. These interactions become important when the accuracy in the determination of the position of weakly bound levels reaches a few megahertz (10^{-4} cm^{-1}). Details on such calculations have been discussed in Ref. [32] for the case of Na_2. The coupled channels code used in the present studies is based on Fourier Grid Hamiltonian method [33].

Preliminary coupled channels calculations (CCC) with potential curves determined in single channel fits showed that the shifts of the calculated energy levels with respect to the unperturbed ones, i.e. the eigenvalues of the single potentials, exceed the experimental uncertainty only for $v_{\rm X} \geq 74$ of the $X^1\Sigma^+$ state and $v_a \geq 14$ of the $a^3\Sigma^+$ state. The strongest one is the coupling between the $v_{\rm X} = 76$ of the $X^1\Sigma^+$ state and $v_a = 16$ of the $a^3\Sigma^+$ state in agreement with our experimental observations on the hyperfine structure. For these levels the coupling leads to shifts of the order of 0.02 cm^{-1}. Generally however, although shifted, the whole pattern of the hyperfine splitting is preserved so that the levels can still be classified as singlet and triplet in the studied region.

As a result of CCC and fitting procedure, the potentials listed in the Table 1 were obtained. In order to assess the quality of the fitted potentials, in addition to the experimental data sets sorted separately for transitions to the singlet and the triplet state, a new combined data set was constructed. It contains all transitions to high vibrational levels of both states ($v_{\rm X} \geq 74$ and $v_a \geq 14$). Differences between these selected transition frequencies were calculated not only between the transitions to a given electronic state, as done before, but also differences between transitions to different states were formed. The combined data set contains 555 transition frequencies forming about 3700 differences. The potentials from Table 1 reproduce these differences with a standard deviation $\sigma = 0.0025$ cm^{-1} and a dimensionless standard deviation of $\bar{\sigma} = 0.63$ and they reproduce the total experimental data for the triplet state with $\sigma = 0.0035$ cm^{-1} and $\bar{\sigma} = 0.59$ and for the singlet state with $\sigma = 0.0032$ cm^{-1} and $\bar{\sigma} = 0.73$.

Comparison of the obtained potentials with the *ab initio* ones from Ref. [18] can be seen in Fig. 2.

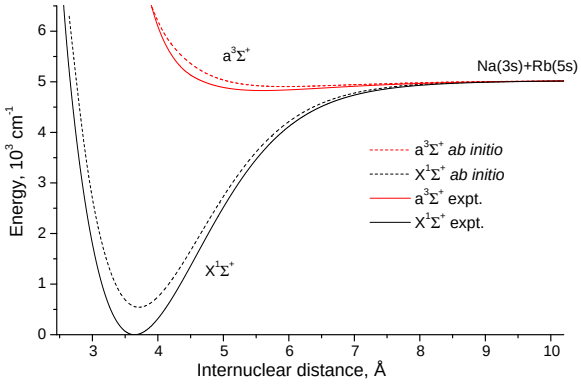

Figure 2. Comparison of the present empirical and *ab initio* [18] potential energy curves.

Results and conclusions

1. New high-resolution LIF data were collected for the $a^3\Sigma^+$ state of NaRb using the FTS method. More than 900 transition frequencies to 490 energy levels were identified. The range of observed vibrational and rotational quantum numbers is $v'' = 1 - 18$ and $N'' = 1 - 80$. The typical experimental uncertainty is 0.003 cm^{-1}.

2. The new vibrational numbering in the $a^3\Sigma^+$ state was established from the isotopic effect in this study: vibrational numbering was changed by +1, compared to the one used in Ref. [21].

3. Data on the high-lying levels of the $a^3\Sigma^+$ and $X^1\Sigma^+$ state were obtained simultaneously using the long-range changeover. The data set for the $X^1\Sigma^+$ state obtained previously (see [dis2]) was correspondingly enriched by about 250 transitions adding some 150 new rovibrational levels. Turning point of the last observed level is ($v''_X = 78$, $J'' = 20$) 15.6 Å being approximate 1 cm^{-1} below the asymptote.

4. Both $X^1\Sigma^+$ and $a^3\Sigma^+$ states potentials were fitted simultaneously to spline-pointwise potential energy curve smoothly connected to the long-range potential, taking into account the hyperfine mixing of these states close to the asymptote. New potentials reproduce experimental frequency differences for the $a^3\Sigma^+$ state with $\sigma = 0.0035$ cm^{-1} and $\bar{\sigma} = 0.59$ and for the $X^1\Sigma^+$ state with $\sigma = 0.0032$ cm^{-1} and $\bar{\sigma} = 0.73$.

5. Long-range coefficients C_6, C_8, C_{10}, as well as exchange energy parameter A_{ex} were fitted. Dispersion potential is in good agreement with the *ab initio* one.

6. New, more precise values of dissociation energies are obtained: $D_e^X = 5030.502$ cm^{-1} and $D_e^a = 203.355$ cm^{-1}. The D_e^a differs significantly from the most recent value from Ref. [31] not only due to the improved experimental data set, but mainly due to the new vibrational assignment established in this study.

7. New potentials allowed reliable predictions of scattering lengthes and Feshbach resonances, necessary for cold collision experiments with Na-Rb pairs.

Table 1. Pointwise representation of the potential energy curves for the $X^1\Sigma^+$ and $a^3\Sigma^+$ states of NaRb.

R [Å]	$U_X(R)$ [cm^{-1}]	R [Å]	$U_X(R)$ [cm^{-1}]
2.100000	23623.67465	5.791989	3880.39592
2.200000	17634.41477	5.973808	4088.60966
2.300000	13279.18859	6.155626	4262.33458
2.400000	10069.56048	6.337444	4405.67319
2.500000	7667.49769	6.519263	4522.91885
2.600000	5874.22172	6.701081	4618.17079
2.700000	4521.74692	6.882899	4695.19866
2.800000	3427.90598	7.064718	4757.28897
2.900000	2528.63531	7.246536	4807.26121
3.000000	1798.65045	7.428355	4847.46365
3.131998	1060.60559	7.610173	4879.81088
3.263996	544.13656	7.791991	4905.89082
3.395993	215.36397	7.973810	4926.95998
3.527991	43.57832	8.155628	4944.02973
3.659989	0.83395	8.499301	4968.08811
3.791987	62.11989	8.699301	4978.43703
3.973805	276.44925	8.899301	4986.78123
4.155624	597.14349	9.192121	4996.27537
4.337442	984.16758	9.514223	5003.97364
4.519260	1405.59678	9.942941	5011.19667
4.701079	1836.47101	10.461689	5016.98016
4.882897	2257.79571	11.152144	5021.73265
5.064716	2655.74803	12.101429	5025.42308
5.246534	3020.92992	13.050715	5027.33721
5.428352	3347.84205	14.000000	5028.47884
5.610171	3634.22011		

R [Å]	$U_a(R)$ [cm^{-1}]	R [Å]	$U_a(R)$ [cm^{-1}]
2.944440	29489.89467	6.468399	4872.49275
3.155560	18461.93317	6.605337	4882.75826
3.366670	12363.70802	6.794944	4896.83178
3.577780	8991.52099	6.984550	4910.34530
3.788890	7126.77387	7.174157	4923.07187
4.000000	6095.47898	7.363764	4934.83385
4.198190	5552.35782	7.553371	4945.59408
4.396380	5237.10044	7.990520	4966.55716
4.594570	5062.99324	8.427668	4982.64596
4.792760	4957.08727	8.864817	4994.72299
4.990949	4890.76470	9.301966	5003.67683
5.189139	4852.15516	9.739114	5010.27403
5.387328	4832.98126	10.176263	5015.16200
5.585518	4827.17289	10.941010	5020.80312
5.783708	4830.40026	11.705758	5024.24404
5.920646	4836.15057	12.470505	5026.30776
6.057584	4843.78306	13.235253	5027.62932
6.194522	4852.68409	14.000000	5028.49121
6.331461	4862.36273		

U_∞=5030.50235 cm^{-1}	
R=11.3370 Å	
C_6=1.3237·10^7 cm^{-1}Å^6	A_{ex}=2.8609·10^4 cm^{-1}Å$^{-\gamma}$
C_8=2.9889·10^8 cm^{-1}Å^8	γ=5.0081
C_{10}=1.5821·10^{10} cm^{-1}Å^{10}	β=2.2085 Å^{-1}
T_e^X = 0 cm^{-1}	R_e^X = 3.6434 Å
D_e^X = 5030.502(50) cm^{-1}	D_o^X = 4977.187(50) cm^{-1}
T_e^a=4827.14727 cm^{-1}	R_e^a=5.6003 Å
D_e^a=203.355(50) cm^{-1}	D_0^a=193.365(50) cm^{-1}

NaRb $C^1\Sigma^+$ state

The Fifth Subchapter contains results of the studies of the $C^1\Sigma^+$ state [dis4]. During the study of the ground state of NaRb, done in Hannover by Fourier-transform spectroscopy of laser-induced fluorescence [dis2], it turned out that a lot of information about the excited $C^1\Sigma^+$ and $D^1\Pi$ states was available from the recorded spectra. Here the first detailed $C^1\Sigma^+$ state analysis based on these experimental data and newly derived data by colleagues from the Institute of Physics and Institute of Experimental Physics in Warsaw is presented.

A single mode, frequency doubled Nd:YAG laser with frequency varied between 18787.25 cm^{-1} and 18788.44 cm^{-1} gave rise to 18 $C^1\Sigma^+ \rightarrow X^1\Sigma^+$ progressions ($v' = 21 - 30$). The Ar^+ ion laser line at 514.5 nm also efficiently excites transitions in the $C^1\Sigma^+ \leftarrow X^1\Sigma^+$ system ($v'= 32 - 44$). Overall, 12 progressions were assigned. The Ar^+ ion laser line 501.7 nm also excites $C^1\Sigma^+ \leftarrow X^1\Sigma^+$ transitions in NaRb, however, the resulting fluorescence was very weak and we were only able to observe it at higher temperatures (620 K). The identified progression originates from $v' = 46$. A term value for $v' = 5$ was obtained from a weak $C^1\Sigma^+ \rightarrow X^1\Sigma^+$ LIF spectrum excited by a Rhodamine 6G dye laser.

Due to the presence of argon buffer gas and very good signal-to-noise ratio several strong fluorescence lines were accompanied by a large number of collisionally-induced rotational satellites from levels ($v', J' \pm \Delta J$) with ΔJ up to 12. The analysis of these satellites has increased the Fourier data set for the $C^1\Sigma^+$ state significantly. It also allowed us to establish a relative numbering of the rovibrational levels of the $C^1\Sigma^+$ state. Overall, from the analysis of the FTS spectra we obtained 138 term values of $Na^{85}Rb$ and 66 of $Na^{87}Rb$ $C^1\Sigma^+$ state with undoubtedly assigned rotational quantum numbers by using the eigenenergies of the ground state potential from Ref. [dis2].

As has been already discussed, e.g. in Ref. [28], by exciting the molecular sample with a single mode laser and by observing the fluorescence in a direction parallel to the laser beam, the resulting fluorescence does not suffer from Doppler broadening. The line frequencies, however, can be shifted from the Doppler-free values within the Doppler profile. As a result, the overall uncertainty of determining the absolute term value from the transition frequencies is generally limited by the Doppler broadening (about 0.03 cm^{-1} FWHM for the typical working temperatures). Therefore we initially adopted the experimental uncertainty value of 0.01 cm^{-1} which was later justified by our data analysis.

From the FTS data a significant portion of the middle part of the C state PEC could be constructed. However, the bottom of the C state was still uncertain, since the main body of measurements ended at $v' = 21$ as the lowest level, with a single measurement on $v' = 5$. In addition, it was important to investigate the possibility for collecting experimental data on the shelf region. Therefore, to enlarge and complete the data, a new experiment using the method of polarization labeling spectroscopy, which is well suited for the studies of the excited states, was performed by our collaborators in Warsaw. Levels in the range $v' = 0 - 64$ were studied with accuracy of 0.05 cm^{-1}. The whole data field available from both Hannover and Warsaw measurements consists of rovibrational levels with $v' = 0 - 64$ and $J' = 4 - 123$.

Due to the special shape of the potential energy curve of the $C^1\Sigma^+$ state we decided to construct a spline-pointwise potential with the IPA method [27]. A use of regularization functional [34] allowed to overcome potential oscillating behavior in the regions poorly determined by the experimental data. The initial guess of the PEC was the difference-based theoretical potential $U_{\rm C}^{dif}(R) = U_{\rm X}^{expt}(R) + \left(U_{\rm C}^{ab\ initio}(R) - U_{\rm X}^{ab\ initio}(R)\right)$.

The final potential describes the experimental term energies of both $Na^{85}Rb$ (1001 levels) and $Na^{87}Rb$ (160 levels) isotopomers. The potential is defined at 49 points and is listed in Table 2. To larger distances a long-range expansion was used

$$U_{\rm LR}(R) = D - \frac{C_6}{R^6} - \frac{C_8}{R^8} - \frac{C_{10}}{R^{10}} \tag{5}$$

with C_6 and C_8 taken from Ref. [35]. D is the energy at the atomic asymptote 21986.672 ± 0.10 cm^{-1}. It was calculated from the Na ($3p_{1/2}$) level energy [36] 16956.1703 cm^{-1} and the value of the ground state dissociation energy $D_e(X^1\Sigma^+) = 5030.50(10)$ cm^{-1} [dis3].

Table 2. List of spline-pointwise potential energy curve grid points for the $C(3)^1\Sigma^+$ state.

R [Å]	$U(R)$ (cm^{-1})	R [Å]	$U(R)$ (cm^{-1})
2.6000	27339.156	5.7188	18627.109
2.7190	25761.642	5.8799	18856.61
2.8380	24277.932	6.0410	19091.257
2.9570	22970.966	6.2020	19326.105
3.0760	21903.509	6.3631	19557.231
3.1950	21024.166	6.5241	19780.173
3.3140	20270.612	6.6852	19990.929
3.4330	19631.429	6.8462	20183.582
3.5519	19105.284	7.0073	20350.56
3.6709	18678.278	7.2342	20519.818
3.7899	18338.747	7.4612	20608.871
3.9089	18075.017	7.6881	20666.835
4.0278	17876.402	7.9151	20728.386
4.1468	17733.865	8.1420	20807.328
4.2658	17639.271	8.5707	21017.979
4.3848	17585.876	8.9993	21330.484
4.5038	17568.111	9.4280	21740.865
4.6228	17581.281	9.8567	21910.956
4.7418	17621.977	10.2853	21950.712
4.8815	17699.64	10.7140	21968.14
5.0209	17805.681	11.1427	21976.325
5.1605	17936.028	11.5700	21980.261
5.3001	18086.687	12.0000	21982.33
5.4397	18254.406	12.4300	21983.475
5.5793	18435.788		
$R_{out} = 12.11009$ Å			
$D = 21986.672$ cm^{-1}		C_8 =2.1416·10^9 cm^{-1}Å^8	
$C_6 = -2.429 \cdot 10^6$ cm^{-1}Å^6		$C_{10} = 9.36942 \cdot 10^9$ cm^{-1}Å^{10}	
Potential minimum			
$R_m = 4.51$ Å		$T_m = 17568.07$ cm^{-1}	

The potential reproduces the polarization labeling spectroscopy data with a standard deviation of 0.037 cm^{-1} and a dimensionless standard deviation of 0.79. The LIF data are reproduced with a standard deviation of 0.0083 cm^{-1} and a dimensionless standard deviation of 0.83. The combined dimensionless standard deviation for both data sets amounts to 0.80.

In Fig. 3 the empirical potential is compared to the *ab initio* potential from Ref. [18] and the difference-based potential. The red line in Fig. 3a displays the difference $\Delta E = U_{\rm C}^{expt} - U_{\rm C}^{dif}$, referring to the magnified right hand side scale, for better visibility, and shows variations of about 100 cm^{-1}. This finding supports the statement from Ref. [4] and suggests that when possible for more reliable predictions it is better to use the differences of *ab initio* potential curves with respect to an experimental potential known with high reliability.

Results and conclusions

1. NaRb $C^1\Sigma^+ \rightarrow X^1\Sigma^+$ high-resolution LIF spectra were obtained for the first time using the FTS method. The data field of the $C^1\Sigma^+$ state has been enlarged significantly by the term values obtained from the analysis of the rotational relaxation lines. Experimental term value uncertainty is 0.01 cm^{-1}.

2. From the analysis of the FTS spectra 138 term values of $Na^{85}Rb$ and 66 term values of $Na^{87}Rb$ $C^1\Sigma^+$ state in the range $v' = 5; 21 - 46$, $J' = 4 - 123$ were obtained.

3. FTS term energies together with the data obtained by our collaborators in Warsaw by polariza-

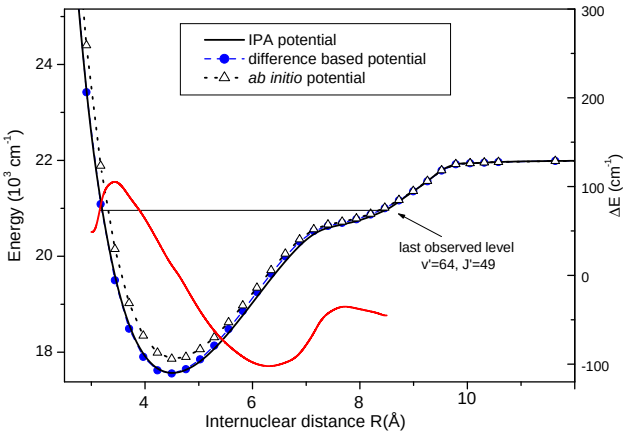

Figure 3. Comparison of the experimental IPA potential for the $C^1\Sigma^+$ state (solid line) and the corresponding *ab initio* potential by Korek *et al.* [18] (triangles and dotted line) and the difference-based potential (full circles). In red: $\Delta E = U_C^{expt} - U_C^{dif}$, referred to the right hand scale.

tion labeling spectroscopy technique were incorporated into a direct fit of a single spline-pointwise potential energy curve to the level energies. The PEC describes the experimental term energies of both $Na^{85}Rb$ (1001 level) and $Na^{87}Rb$ (160 levels) isotopomers with $\sigma = 0.037$ cm^{-1} and $\bar{\sigma} = 0.80$. The FTS data are reproduced with $\sigma = 0.0083$ cm^{-1} and $\bar{\sigma} = 0.83$.

4. Dissociation energy of the $C^1\Sigma^+$ state obtained with the present potential is 4418.6 ± 0.3 cm^{-1}.

5. Term energies were also fitted to Dunham expansion below the "shelf region". The obtained set of constants reproduces the experimental term energies in the range $0 \le v' \le 40$ and $8 \le J' \le 121$ with $\bar{\sigma} = 0.92$.

NaRb $D^1\Pi$ state

The Sixth Subchapter deals with the studies of the $D^1\Pi$ state [dis5]. Analysis based on D → X LIF data and rotational relaxation lines is presented. Detailed analysis of the observed Λ-doubling for various rovibrational levels is also given.

The Ar^+ laser 514.5, 501.7, 496.5, 488.0, and 476.5 nm laser lines efficiently induced the D→X fluorescence in NaRb. Overall 130 progressions were assigned ($v' = 0 - 39$). A tunable single mode, frequency doubled Nd:YAG laser was also used to excite $D^1\Pi \leftarrow X^1\Sigma^+$ transitions in NaRb. The laser frequency was varied between 18787.25 cm^{-1} and 18788.44 cm^{-1} giving rise to 38 D→X progressions ($v' = 0 - 16$).

Due to the presence of the argon buffer gas and very good signal-to-noise ratio some strong fluorescence lines were accompanied by a large number of collisionally-induced satellites with ΔJ up to ±30. The analysis of rotational satellites has enlarged the data set of the $D^1\Pi$ state significantly. The experimental uncertainty value of 0.01 cm^{-1} was adopted similarly to the case of the $C^1\Sigma^+$ state.

The $D^1\Pi \rightarrow X^1\Sigma^+$ rotational relaxation spectra appeared due to collisional population of neighboring rotational levels in the $D^1\Pi$ state preferably with the same symmetry (e or f) and subsequent D-X emission according to selection rules for electric dipole transitions. However, in a number of cases the strongest LIF lines had additional satellites coming from the neighboring rotational levels of the opposite symmetry. Thus, a strong Q line had not only a Q satellite branch, but also the P and R satellites. This opened the opportunity to establish directly the Λ-splitting of rotational levels of the $D^1\Pi$ state. From

the analysis of the Q lines we obtained f level energies, whereas from the analysis of the P and R lines we obtained the energies of e levels. Then the evaluation of q factors is straightforward:

$$E_e - E_f = \Delta_{e/f} = qJ'(J'+1). \tag{6}$$

This allowed us to obtain q factor values and their sign for 20 vibrational levels in the interval $v' = 0 - 35$ in a wide range of rotational quantum numbers ($J' = 20 - 122$). For most of the vibrational levels q factors are around $0.9 \cdot 10^{-5}$ cm^{-1}. In few cases an anomalous behavior of the Λ-splittings was observed, clearly indicating a local perturbation in the $D^1\Pi$ state. Analysis of q factors outside the local perturbation regions in $v' = 0 - 30$ range did not reveal a vibrational or isotopomer dependence within our accuracy, whereas a slight decrease of q factors with J' was observed. Thus it was possible to describe the whole set of q factors by one J'-dependence

$$q = q_0 + q_1 J'. \tag{7}$$

The resulting fit parameters in (7) are $q_0 = 1.079(14) \cdot 10^{-5}$ cm^{-1} and $q_1 = -2.30(15) \cdot 10^{-8}$ cm^{-1}.

The q factors measured in this work are consistent with the radiofrequency-optical double resonance measurements [4], which are of higher accuracy, but cover a very limited set of measured levels with $J' \leq 52$. The calculated q factors [4] are in good agreement with the experimental data, but slightly larger, probably because of neglecting the influence of the $^1\Sigma^+$ states higher than the $E^1\Sigma^+$ state in the calculations.

The $D^1\Pi$ state for both isotopomers of NaRb is described in the adiabatic approximation with a single potential energy curve. The potential was defined as proposed in Ref. [27] as a set of points $\{R_i, U(R_i)\}$ connected by cubic spline functions. Fitting procedure is similar to that used for the NaRb $C^1\Sigma^+$ state. As initial guess for the potential curve we took the RKR potential constructed using molecular constants from Ref. [4]. Since the shift of the f levels under the influence of higher Σ^- states is expected to be very small, the potential fit was based on the f levels considered as "unshifted". The e levels were also included in the fit after subtracting from their experimental term energies the value of the Λ-splitting $q(J')J'(J'+1)$. Levels showing deviations more than 0.03 cm^{-1} (7% of the whole data set) were not included in the final fitting procedure, these levels are considered either as perturbed or as Doppler shifted levels. Taking into account the $q(J')$ dependence of Eq. (7), the final potential fits all unperturbed energy levels of both isotopomers with a standard deviation of 0.008 cm^{-1} and a dimensionless standard deviation of 0.78. It consists of 35 points and is given in Table 3. Note, that if the J' dependence of the q factors is neglected and a single averaged q factor ($0.87 \cdot 10^{-5}$ cm^{-1}) is used, we get a standard deviation of 0.009 cm^{-1} and a dimensionless standard deviation of 0.88.

Initially, the PEC was constructed in a pointwise form up to 10 Å. In order to ensure the proper asymptotic behavior of the potential we connected the PEC with a long-range (LR) branch, for which we adopted the usual dispersion form (5) with coefficients C_6 and C_8 taken from Ref. [35]. The dissociation asymptote D of the $D^1\Pi$ state correlating to the Na($3p_{3/2}$) + Rb($5s_{1/2}$) atomic limit was calculated from the Na($3p_{3/2}$) level energy [36] and the $X^1\Sigma^+$ state dissociation energy 5030.50(10) cm^{-1} [dis3]. The connecting point R_{out} and the C_{10} parameter were varied in order to ensure a smooth connection with the pointwise potential. Thus, the C_{10} parameter presented here should be considered as an effective coefficient only.

In Figure 4a the experimental IPA potential is compared with the *ab initio* potential from Ref. [18] (full circles). Also the difference-based potential $U_D^{dif}(R) = U_X^{expt}(R) + \left(U_D^{ab\ initio}(R) - U_X^{ab\ initio}(R)\right)$. suggested in Refs. [4, 37] as an improved estimate from *ab initio* results is given in Figure 4a (open circles). As can be seen, the difference-based potential is much closer to the IPA potential than the *ab initio* one. Similar conclusions were obtained in studies of the NaRb $A^1\Sigma^+ - b^3\Pi$ complex in Ref. [37] and by present studies of the NaRb $C^1\Sigma^+$ state [dis4]. The difference between the IPA potential and the RKR potential from Ref. [4] is shown in Fig. 4b.

We have measured a number of v', J' levels whose experimental term values deviate from the calculated ones by more than 0.03 cm^{-1} indicating a possible presence of local perturbations. We have found more than 10 perturbation regions in the $v' = 0-39$ interval. Perturbations are caused by nearby triplet states,

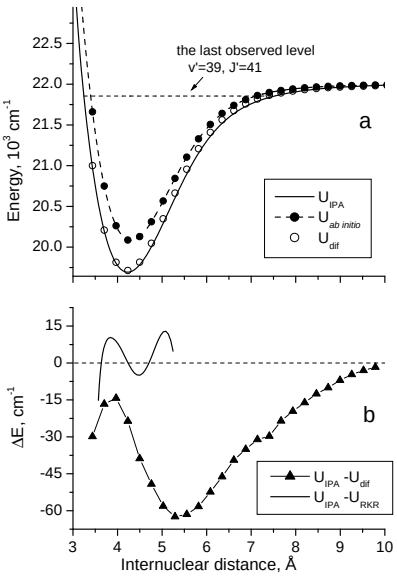

Figure 4. (a) Comparison of the new determination of the $D^1\Pi$ state IPA potential (solid line) with the corresponding *ab initio* potential by Korek *et al.* [18] (full circles) and the difference-based potential (open circles), moved to the correct atomic limit (b) Difference of the IPA potential $U_{\rm IPA}$ with respect to the difference-based potential (triangles) and to the RKR potential $U_{\rm RKR}$ from Ref. [4] (solid line).

Table 3. List of the grid points of the potential energy for the NaRb $D^1\Pi$ state. Energies are given with respect to the minimum of the ground state.

R [Å]	$U(R)$ (cm^{-1})	R [Å]	$U(R)$ (cm^{-1})
2.80000	26088.574	5.28571	20599.728
2.97500	23892.559	5.42857	20762.635
3.15000	22416.175	5.57143	20916.356
3.32500	21452.447	5.71429	21058.223
3.50000	20753.769	5.85714	21186.491
3.60000	20448.239	6.00000	21300.660
3.70000	20203.231	6.29429	21491.459
3.80000	20013.336	6.58857	21630.673
3.90000	19872.445	6.88286	21729.052
4.00000	19775.498	7.17714	21798.073
4.14286	19703.369	7.64762	21870.204
4.28571	19697.224	8.11810	21915.936
4.42857	19744.947	8.58857	21945.594
4.57143	19835.458	9.05905	21964.683
4.71429	19958.393	9.52952	21977.465
4.85714	20104.327	9.86476	21984.053
5.00000	20264.751	10.20000	21989.488
5.14286	20432.036		
$R_{out} = 9.94559$ Å			
$D = 22003.868$ cm^{-1}		$C_8 = 3.4178 \cdot 10^9$ cm^{-1}Å^8	
$C_6 = -1.5046 \cdot 10^7$ cm^{-1}Å^6		$C_{10} = -1.6265 \cdot 10^{10}$ cm^{-1}Å^{10}	
Potential minimum			
$R_m = 4.2279$ Å		$T_m = 19692.564$ cm^{-1}	

apparently the $d^3\Pi$ or the $e^3\Sigma^+$. For higher vibrational levels the additional influence of the $E^1\Sigma^+$ state cannot be excluded.

Results and conclusions

1. NaRb $D^1\Pi \rightarrow X^1\Sigma^+$ high-resolution LIF spectra were obtained for the first time using the FTS method. The data field of the $D^1\Pi$ state has been enlarged significantly by the term values obtained from the analysis of the rotational relaxation lines. Experimental term value uncertainty is 0.01 cm^{-1}.

2. From the analysis of the FTS spectra 1182 term values of $Na^{85}Rb$ and 314 term values of $Na^{87}Rb$ for the $D^1\Pi$ state were obtained. The range of vibrational and rotational quantum numbers is $v' = 0 - 39$ and $J' = 1 - 200$. The present FTS measurements characterize 93.5% of the $D^1\Pi$ state potential well.

3. A large set of q factors in the $D^1\Pi$ state was obtained allowing one to derive their dependence on the rotational quantum number J'. No vibrational dependence of q factors was observed within the accuracy of present measurements. In several cases an anomalous behavior of a q factor was observed, clearly indicating a local perturbation in the $D^1\Pi$ state.

4. Experimental term energies were incorporated into a direct fit of a single spline-pointwise potential energy curve to the level energies. The PEC describes the experimental term energies of both NaRb isotopomers with $\sigma = 0.008$ cm^{-1} and $\bar{\sigma}$ =0.78.

5. Dissociation energy of the $D^1\Pi$ state obtained with the present potential is 2311.30 ± 0.14 cm^{-1}.

6. Term energies were also represented by a Dunham expansion. The obtained set of constants reproduces the experimental term energies in $\sigma = 0.009$ cm^{-1} and a dimensionless standard deviation of $\bar{\sigma} = 0.87$ for both isotopomers.

7. Analysis of perturbation regions revealed that both e and f components are perturbed, thus testifying to the triplet character of perturbing state. Apparently, either the $d^3\Pi$ or the $e^3\Sigma^+$ state perturbs the $D^1\Pi$ state.

NaCs molecule

The Fifth Chapter contains research results on the NaCs $X^1\Sigma^+$ and $a^3\Sigma^+$ states. **The First Subchapter** describes the existing literature data on NaCs. Accurate experimental spectroscopic information on NaCs is still limited, including that for the ground state. Therefore the **goal** to study the ground $X^1\Sigma^+$ and lowest triplet $a^3\Sigma^+$ states of NaCs was introduced.

NaCs $X^1\Sigma^+$ state

The Second Subchapter describes analysis of the NaCs $X^1\Sigma^+$ state [dis6]. Strong LIF was observed when the sample was illuminated with Ar^+ laser operated at lines: 514.5, 496.5, 488.0, 476.5 nm (single mode) and by a single mode dye laser with Rhodamine 6G dye. This allowed us to observe the $(3)^1\Pi - X^1\Sigma^+$, $(2)^1\Pi - X^1\Sigma^+$ and $(4)^1\Sigma^+ - X^1\Sigma^+$ transitions in NaCs. Ar^+ lines 514.5 and 496.5 nm excited the $(3)^1\Pi - X^1\Sigma^+$ and $(4)^1\Sigma^+ - X^1\Sigma^+$ transitions in NaCs. Ar^+ lines 488.0 and 476.5 nm excited only the $(3)^1\Pi$ state. Overall 55 $(3)^1\Pi - X^1\Sigma^+$ and 14 $(4)^1\Sigma^+ - X^1\Sigma^+$ progressions were assigned. The frequency of the Rhodamine 6G laser was varied between 17527 cm^{-1} and 17768 cm^{-1} which allowed us to record and assign about 40 $(2)^1\Pi \rightarrow X^1\Sigma^+$ and 10 $(4)^1\Sigma^+ \rightarrow X^1\Sigma^+$ progressions. Due to a considerable extension of the $(4)^1\Sigma^+$ potential in internuclear separation, see Fig. 1*b*, it was possible to observe transitions to high vibrational levels of the ground state (up to $v'' = 83$) close to the dissociation limit. The assignment of the recorded spectra was simplified by the published $X^1\Sigma^+$ state RKR potential in

Ref. [38]. The total data set consists of more than 5070 transitions corresponding to 2892 different ground state levels in NaCs.

For the construction of ground state PEC we used both spline-pointwise and analytic potentials. Analytic potential suggested in Ref. [32] is represented as a truncated expansion over analytic functions, where fitting parameters are a_i. This analytic form is used in the interval $R_i < R < R_o$:

$$U(R) = \sum_{i=0}^{n} a_i \left(\frac{R - R_m}{R + bR_m} \right)^i . \tag{8}$$

For the region $R \geq R_o$ the long-range expression is applied:

$$U_{\rm LR}(R) = D_e - \frac{C_6}{R^6} - \frac{C_8}{R^8} - \frac{C_{10}}{R^{10}} - E_{ex}, \tag{9}$$

where exchange energy $E_{ex}{=}A_{ex}R^{\gamma}\exp(-\beta R)$. Parameters β and γ are estimated from the atomic ionization energies of Na and Cs [39]. C_6, C_8 and C_{10} were fixed to their most recent theoretical values from Refs. [30, 29]. D_e and A_{ex} were fitted. R_m, b and the connecting points R_i and R_o were kept fixed to values, which allow fast convergence of the fitting routine.

For short internuclear distances $R \leq R_i$ the potential is smoothly extended with the expression:

$$U_{\rm SR}(R) = A\exp(-B(R - R_i)), \tag{10}$$

where A and B were adjusted in order to ensure smooth connection between the extension and the analytic form.

According to Eq. (8), 29 potential coefficients were used for the fit, which allowed us to fit almost all observations within experimental accuracy. Only levels with a turning point around 12 Å or larger showed systematic deviations, which, as follows from the later experiments and analysis, are ascribed to the mixing of the singlet and triplet states.

Spline-pointwise potential was constructed similarly to the NaRb $X^1\Sigma^+$ state case. The final potential contains 51 points. Note, that in the case of spline-pointwise potential the contribution of the exchange energy is incorporated into the C_{10}/R^{10} term, thus C_{10} being an effective parameter.

Results and conclusions

1. High-resolution LIF spectra to the NaCs $X^1\Sigma^+$ ground state were obtained for the first time using the FTS method. The obtained data set consists of more than 5070 transitions corresponding to 2892 different ground state levels in the range $v' = 0 - 83$, $J' = 2 - 179$.

2. Transition frequencies were used for a direct fit of the analytic and spline-pointwise potential energy curves. Analytic potential (29 parameters) reproduces experimental data with $\sigma = 0.003$ cm^{-1} and $\bar{\sigma} = 0.88$, whereas spline-pointwise PEC (51 parameters) with $\sigma = 0.0029$ cm^{-1} and $\bar{\sigma} = 0.61$.

3. Experimental PEC covers 99.97% of the potential well depth. The classical turning point of the last observed energy level ($v'' = 83$, $J'' = 12$) is around 15.3 Å and this level is about 1.4 cm^{-1} below the asymptote.

4. A new, more accurate value of dissociation energy is obtained with the present potential $D_e = 4954.18 \pm 0.10$ cm^{-1}.

5. Term energies were also fitted to the Dunham expansion. Obtained set of constants reproduces the experimental term energies with $\sigma = 0.0027$ cm^{-1} and $\bar{\sigma} = 0.73$.

Table 4. Parameters of the analytic representation (Eqs. 8, 9, 11) of the potential energy curve of the $a^3\Sigma^+$ state in NaCs. Potential is given with respect to the atomic asymptote.

for $R \leq 4.78$ Å	
A	-0.164777827×10^3 cm^{-1}
B	$0.184208874 \times 10^{19}$ cm^{-1}Å$^{\alpha}$
α	0.236563805×10^2
for 4.78 Å $< R <$ 10.20 Å	
b	-0.6400
R_m	5.75585938 Å
a_0	-217.137992 cm^{-1}
a_1	5.060041760921147 cm^{-1}
a_2	$0.4718687621656754 \times 10^3$ cm^{-1}
a_3	$0.2514219323834187 \times 10^3$ cm^{-1}
a_4	$-0.8746237247738273 \times 10^2$ cm^{-1}
a_5	$-0.2154118954152781 \times 10^3$ cm^{-1}
a_6	$-0.2370010651661931 \times 10^3$ cm^{-1}
a_7	$-0.5975533223022640 \times 10^3$ cm^{-1}
a_8	$-0.4760140339369856 \times 10^3$ cm^{-1}
a_9	$0.3782291928282492 \times 10^3$ cm^{-1}
a_{10}	$0.6798234616502023 \times 10^3$ cm^{-1}
a_{11}	$0.6723220594269379 \times 10^3$ cm^{-1}
a_{12}	$-0.1248173837589433 \times 10^2$ cm^{-1}
a_{13}	$-0.4626112296933644 \times 10^3$ cm^{-1}
for $R \geq 10.20$ Å	
C_6	1.545671×10^7 cm^{-1}Å^6
C_8	5.001807×10^8 cm^{-1}Å^8
C_{10}	2.019156×10^{10} cm^{-1}Å^{10}
A_{ex}	2.549387×10^4 cm^{-1}Å$^{-\gamma}$
γ	5.12271
β	2.17237 Å^{-1}
T_e=$-D_e$	$-217.152(10)$ cm^{-1}
R_e	5.745 Å

Combined analysis of the NaCs $a^3\Sigma^+$ and $X^1\Sigma^+$ states

The Third Subchapter is devoted to the combined analysis of the $a^3\Sigma^+$ and $X^1\Sigma^+$ states of NaCs. The lowest triplet state of NaCs has never been studied experimentally before. Therefore the **goal** of the present experiments was to collect experimental information on the NaCs $a^3\Sigma^+$ state, especially close to the asymptote and to perform a combined analysis of the $a^3\Sigma^+$ and $X^1\Sigma^+$ states, taking into account their hyperfine mixing.

In order to study the $a^3\Sigma^+$ state we excited with a dye laser (DCM dye) transitions to levels of the $B^1\Pi$, $b^3\Pi$ and $c^3\Sigma^+$ complex and observed emission to the $X^1\Sigma^+$ and $a^3\Sigma^+$ states. The frequency of the DCM laser was gradually varied between 14966 cm^{-1} and 15882 cm^{-1}. The lowest frequency at which triplet band appeared was ca. 15145 cm^{-1}. As a result, we have obtained the data set for the $a^3\Sigma^+$ state consisting of more than 3000 transition frequencies to ca. 940 energy levels. Uncertainty was estimated to be 0.003 cm^{-1}. The range of observed vibrational and rotational quantum numbers is $6 < N'' < 103$, $0 < v'' < 19$. The last observed level is $v'' = 19$, $N'' = 25$, which has a classical turning point around 14.2 Å.

In our experiments we observed several spectra where the long-range changeover effects are noticeable, similarly to the NaRb case [dis3]. Thus transitions to high vibrational levels of the $X^1\Sigma^+$ state were found together with the $a^3\Sigma^+$ transitions and enriched the data field of the $X^1\Sigma^+$ state. However these spectra were rare and the highest v'' did not exceed the previously reached $v_X = 83$.

At the resolution used in the experiments (typically 0.015-0.03 cm^{-1}) the hyperfine structure (HFS) of the triplet lines was partially resolved. Analysis showed that the hyperfine splitting of the $a^3\Sigma^+$ levels is described within a Hund's case ($b_{\beta S}$) coupling scheme and is caused by the Fermi contact interaction like in the $a^3\Sigma^+$ state of NaRb. The observed structure is well described by atomic HFS parameters for

Table 5. Parameters of the analytic representation (Eqs. 8, 9, 11) of the potential energy curve of the $X^1\Sigma^+$ state in NaCs. Potential is given with respect to the atomic asymptote.

for $R \leq 2.84$ Å	
A	0.900290886×10^4 cm^{-1}
B	-0.113527906×10^3 cm^{-1}Å$^{\alpha}$
α	-4.1859263636
for 2.84 Å $< R <$ 10.20 Å	
b	-0.4000
R_m	3.85062906 Å
a_0	-4954.220839 cm^{-1}
a_1	0.8980684901406436 cm^{-1}
a_2	$0.1517322305891121 \times 10^5$ cm^{-1}
a_3	$0.1091020368289819 \times 10^5$ cm^{-1}
a_4	$-0.2458305183215540 \times 10^4$ cm^{-1}
a_5	$-0.1608232304418994 \times 10^5$ cm^{-1}
a_6	$-0.8705013039210540 \times 10^4$ cm^{-1}
a_7	$0.2188050377166237 \times 10^5$ cm^{-1}
a_8	$-0.3002538567610332 \times 10^6$ cm^{-1}
a_9	$-0.7869349465616797 \times 10^6$ cm^{-1}
a_{10}	$0.3396165702257235 \times 10^7$ cm^{-1}
a_{11}	$0.7358409821995481 \times 10^7$ cm^{-1}
a_{12}	$-0.2637478410754801 \times 10^8$ cm^{-1}
a_{13}	$-0.4458510218550479 \times 10^8$ cm^{-1}
a_{14}	$0.1351336683210848 \times 10^9$ cm^{-1}
a_{15}	$0.1762627711656325 \times 10^9$ cm^{-1}
a_{16}	$-0.4756878196895964 \times 10^9$ cm^{-1}
a_{17}	$-0.4474883318729266 \times 10^9$ cm^{-1}
a_{18}	$0.1216000437575875 \times 10^{10}$ cm^{-1}
a_{19}	$0.7460756869348375 \times 10^9$ cm^{-1}
a_{20}	$-0.2291733580746639 \times 10^{10}$ cm^{-1}
a_{21}	$-0.8708937018563435 \times 10^9$ cm^{-1}
a_{22}	$0.3095441525806588 \times 10^{10}$ cm^{-1}
a_{23}	$0.8199544778248683 \times 10^9$ cm^{-1}
a_{24}	$-0.2806754519640437 \times 10^{10}$ cm^{-1}
a_{25}	$-0.6963731310931557 \times 10^9$ cm^{-1}
a_{26}	$0.1516535914525204 \times 10^{10}$ cm^{-1}
a_{27}	$0.4445582767694474 \times 10^9$ cm^{-1}
a_{28}	$-0.3669909023138414 \times 10^9$ cm^{-1}
a_{29}	$-0.1352434700004024 \times 10^9$ cm^{-1}
for $R \geq 10.20$ Å	
C_6	1.545671×10^7 cm^{-1}Å^6
C_8	5.001807×10^8 cm^{-1}Å^8
C_{10}	2.019156×10^{10} cm^{-1}Å^{10}
A_{ex}	2.549387×10^4 cm^{-1}Å$^{-\gamma}$
γ	5.12271
β	2.17237 Å^{-1}
T_e=$-D_e$	$-4954.221(10)$ cm^{-1}
R_e	3.851 Å

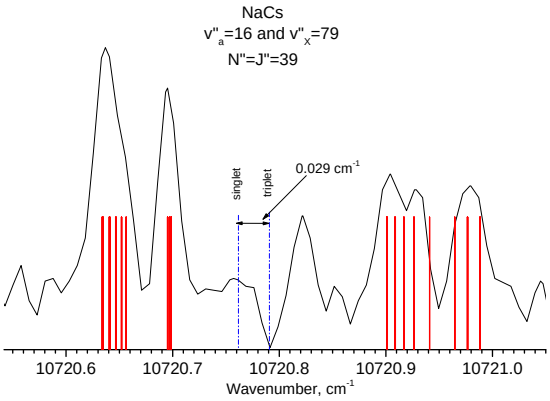

Figure 5. Hyperfine mixing of weakly bound singlet ($v''_{\rm X} = 79$) and triplet ($v''_a = 16$) levels with $N''_a = J''_X = 39$. Solid red lines show the eigenvalues obtained with the CCC with the present potentials, and dashed blue lines denote the single-channel eigenenergies.

levels not close to the asymptote

Altogether ca. 9500 frequencies corresponding to app. 4700 energy levels of both a and X states were used in the combined fitting procedure of obtaining analytic potential energy curves (8). For the long-range region $R \geq R_o$ the expression (3) is applied with some modification: in the present studies potential is given with respect to the atomic asymptote, therefore D is set to 0. C_6, C_8 and C_{10} coefficients and exchange energy parameter A_{ex} were fitted. Parameters β and γ are estimated as discussed for heteronuclear species in [39] from the atomic ionization energies of Na and Cs. For short internuclear distances $R \leq R_i$ the potential is smoothly extended with the expression:

$$U_{\rm SR}(R) = A + B/R^{\alpha}, \tag{11}$$

where α can be non-integer.

The derived potentials describe the total data set of the X and a state with a normalised standard deviation of 0.78. The importance of applying the coupled channels approach can be illustrated with the example of transitions to $v''_a = 16$ and $v''_{\rm X} = 79$, see Fig. 5. The hyperfine coupling of the X and a state levels is so strong that classification of levels as singlets and triplets becomes ambiguous, which is confirmed by the spin operator expectation values, which value for several HFS components is about 0.5. As can be inferred from Fig. 5 coupled channels approach allows for reproducing of the observed HFS pattern with good accuracy.

The obtained dispersion coefficients are in good agreement with theoretical calculations from Refs. [29, 30]. Empirical potentials were compared with *ab initio* potentials by Korek *et al.* [19], see Fig. 6. We can see that in the case of NaCs *ab initio* potentials of the a and X states are much closer to the empirical ones than it was in NaRb (compare with Fig. 2). Quantitatively it is also indicated by *ab initio* dissociation energy values (214 cm^{-1} for a state and 4923 cm^{-1} for X state) that are close to the experimental ones.

Results and conclusions

1. Transitions to the $a^3\Sigma^+$ state of NaCs were observed for the first time. Spectra were recorded using high-resolution FTS. More than 3000 transition frequencies to ca. 940 energy levels were assigned. The range of observed vibrational and rotational quantum numbers is $v'' = 0-19$ and $N'' = 6-103$. The typical experimental uncertainty is 0.003 cm^{-1}.

2. The data set for the $X^1\Sigma^+$ state obtained previously (see [dis6]) was enriched by about 1350 transitions, using B$\rightarrow$X, $(4)^1\Sigma^+ \rightarrow X^1\Sigma^+$ bands and transitions caused by the long-range changeover.

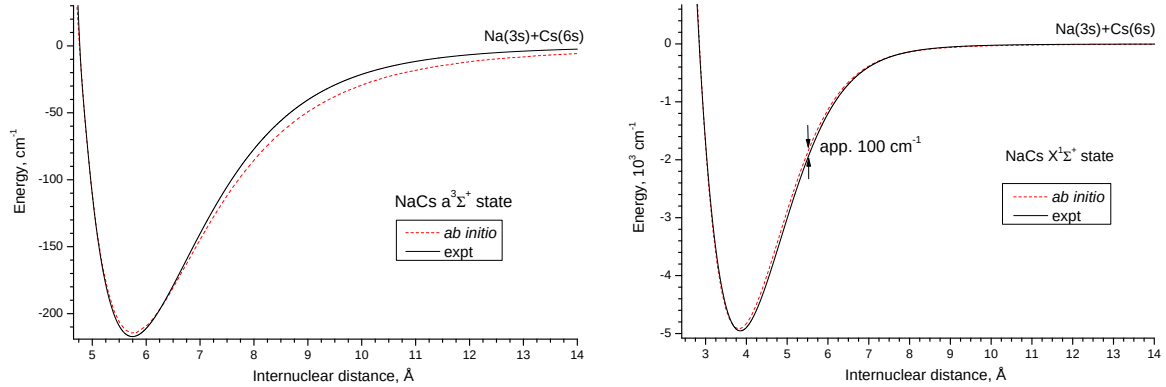

Figure 6. Comparison of the present empirical NaCs $a^3\Sigma^+$ and $X^1\Sigma^+$ state potentials with *ab initio* potentials from Ref. [19].

3. Both $X^1\Sigma^+$ and $a^3\Sigma^+$ states potentials were fitted simultaneously to analytic potential energy curves smoothly connected to the long-range potential, taking into account the hyperfine mixing of these states close to the asymptote. New potentials reproduce experimental data for the $a^3\Sigma^+$ and $X^1\Sigma^+$ state with $\bar{\sigma} = 0.78$.

4. Long-range coefficients C_6, C_8, C_{10}, as well as exchange energy parameter A_{ex} were fitted. Dispersion potential is in good agreement with the *ab initio* one.

5. Dissociation energies obtained with the present potentials for the $X^1\Sigma^+$ and $a^3\Sigma^+$ states are $D_e^X = 4954.22 \pm 0.10$ cm^{-1} and $D_e^a = 217.15 \pm 0.10$ cm^{-1}.

Results and conclusions of the Thesis

In consistence with the goals and tasks of the present work the following **main results** have been obtained:

- For the first time the NaRb ground $X^1\Sigma^+$ state and lowest triplet $a^3\Sigma^+$ state have been studied experimentally in a wide range of internuclear distances with high accuracy. Spline-pointwise empirical potential energy curves were obtained in a combined fitting procedure taking into account the hyperfine mixing of these states close to the asymptote. The obtained potentials allow for adequate modeling of cold collision experiments with Na-Rb pairs.

- A first detailed experimental study of the NaRb excited $C^1\Sigma^+$ state converging to the Na(3p) + Rb(5s) states of separated atoms has been performed. The obtained data were incorporated into a direct fit of a single spline-pointwise potential energy curve to the level energies. This method allowed for description of this state including the shelf region.

- A detailed experimental study of the NaRb $D^1\Pi$ state converging to the Na(3p) + Rb(5s) atomic limit has been performed for the first time with high resolution. The obtained data were incorporated into a direct fit of a single spline-pointwise potential energy curve to the level energies. The $D^1\Pi$ state q factors, which describe the Λ-doubling, have been obtained in a wide range of rotational and vibrational quantum numbers. The rotational dependence of q-factors has been derived. Analysis revealed several local perturbation regions in the $D^1\Pi$ state.

- For the first time the NaCs ground $X^1\Sigma^+$ state has been studied experimentally in a wide range of internuclear distances with high accuracy. The lowest triplet $a^3\Sigma^+$ state has been observed for the first time and studied at high resolution in a wide range of internuclear distances. Analytical empirical potential energy curves of the $X^1\Sigma^+$ and $a^3\Sigma^+$ states were obtained in a combined fitting procedure taking into account the hyperfine mixing of these states close to the asymptote.

Concluding remarks

- Our work has demonstrated that Fourier transform spectroscopy of laser induced fluorescence is a powerful tool for studying not only of ground states, but also excited states due to collision induced transitions. Analysis of rotational satellites allows enlarging of the data sets significantly. In this sense collision facilitated FTS LIF method can be considered for excited states as a method, competing and complementary to two laser pump-probe spectroscopy experiments. Its main advantages are relative easiness of the experiment, high accuracy and fast measurements.

- Applying of direct potential fit analysis allowed us to obtain empirical potential energy curves from the observations. This fully quantum mechanical approach allows to represent the experimental data with equivalent accuracy compared to conventional analysis based on fits to empirical level energy expressions, but at the same time provides us with much better physical model of the electronic state.

- Analysis of the ground and lowest triplet state of NaRb and NaCs highlighted the importance of taking into account the hyperfine mixing of weakly bound levels of these states near the asymptote for providing the proper long-range description.

- Comparison of the derived empirical potentials of the ground and selected excited states of NaRb and NaCs with the *ab initio* data allowed us to conclude that accuracy of *ab initio* potential energy curves is growing over the years, but measurements are still necessary for meeting the demands of modern spectroscopy tasks in the short-range region. Analysis showed that for more reliable predictions of excited state potentials in many cases it is better to use the differences of *ab initio* potential energy curves with respect to the ground state potential, if it is known with high accuracy.

On the other hand, *ab initio* long-range potentials are of much higher accuracy and show agreement with the experiment consistent with the reported experimental and *ab initio* uncertainties.

- The results obtained in the course of work open path for new experimental studies, e.g. dynamic and structural studies of these molecules (measurements of lifetimes, permanent electric dipole moments, etc.) and cold collision experiments with atomic pairs.

References

[1] E. Wiedemann and G.C. Schmidt, Ann. Physik 42, 448 (1891).

[2] G. Herzberg, Molecular Spectra and Molecular Structure. I. Spectra of Diatomic Molecules, D. Van Nostrand Company, New York, Second Edition, 1953.

[3] C.H. Townes, A.L. Schawlow, Microwave Spectroscopy, McGraw-Hill, New York, 1955.

[4] A. Zaitsevskii, S.O. Adamson, E.A. Pazyuk, A.V. Stolyarov, O. Nikolayeva, O. Docenko, I. Klincare, M. Auzinsh, M. Tamanis, R. Ferber, and R. Cimiraglia, Phys. Rev. A 63, 052504 (2001).

[5] H. Lefebvre-Brion and R. W. Field, Perturbations in the Spectra of Diatomic Molecules, Academic, New York, London, 1986.

[6] Special issue on Cold molecules, Eur. Phys. J. D 31, 149 (2004).

[7] D. J. Heinzen, R. Wynar, P. D. Drummond, and K. V. Kheruntsyan, Phys. Rev. Lett. 84, 5029 (2000).

[8] M. G. Kozlov and D. DeMille, Phys. Rev. Lett. 89, 133001 (2002).

[9] J. J. Hudson, B. E. Sauer, M. R. Tarbutt, and E. A. Hinds, Phys. Rev. Lett. 89, 023003 (2002).

[10] D. DeMille, Phys. Rev. Lett. 88, 067901 (2002).

[11] J.T. Bahns,W.C. Stwalley, P.L. Gould, Adv. At. Mol. Opt. Phys. 42, 171 (2000).

[12] F. Masnou-Seeuws, P. Pillet, Adv. At. Mol. Opt. Phys. 47, 53 (2001).

[13] C.A. Moore, G.P. Davis, R.A. Gottscho, Phys. Rev. Lett. 52, 538 (1984).

[14] M. Auzinsh, R. Ferber, O. Nikolayeva, N. Shafer-Ray, M. Tamanis, J. of Phys. D: Applied Physics 34, 624 (2001).

[15] G. D. Telles, L. G. Marcassa, S. R. Muniz, S. G. Miranda, A. Antunes, C. Westbrook, and V. S. Bagnato, Phys. Rev. A 59, R23 (1999).

[16] Y. E. Young, R. Ejnisman, J. P. Shaffer, and N. P. Bigelow, Phys. Rev. A 62, 055403 (2000).

[17] C. Haimberger, J. Kleinert, M. Bhattacharya, and N. P. Bigelow, Phys. Rev. A 70, 021402(R) (2004).

[18] M. Korek, A.R. Allouche, M. Kobeissi, A. Chaalan, M. Dagher, K. Fakherddin, M. Aubert-Frecon, Chem. Phys. 256, 1 (2000).

[19] M. Korek, A. R. Allouche, K. Fakhreddine, and A. Chaalan, Can. J. Phys. 78, 977 (2000).

[20] S. Kasahara, T. Ebi, M. Tanimura, H. Ikoma, K. Matsubara, M. Baba, and H. Katô, J.Chem. Phys. 105, 1341 (1996).

[21] Y-C. Wang, M. Kajitani, S. Kasahara, M. Baba, K. Ishikawa, and H. Katô, J. Chem. Phys. 95, 6229 (1991).

[22] O. Nikolayeva, I. Klincare, M. Auzinsh, M. Tamanis, R. Ferber, E.A. Pazyuk, A.V. Stolyarov, A. Zaitsevskii, R. Cimiraglia, J. Chem. Phys. 113, 4896 (2000).

[23] P. G. Hajigeorgiou and R. J. Le Roy, J. Chem. Phys. 112, 3949 (2000).

[24] M. Marinescu and H. R. Sadeghpour, Phys. Rev. A. 59, 390 (1999).

[25] Y-C. Wang, K. Matsubara, and H. Katô, J. Chem. Phys., 97, 811 (1992).

[26] N. Takahashi and H. Katô, J. Chem. Phys. 75, 4350 (1981).

[27] A. Pashov, W. Jastrzebski, and P. Kowalczyk, Comput. Phys.Commun. 128, 622 (2000).

[28] O. Allard, A. Pashov, H. Knöckel, and E. Tiemann, Phys. Rev. A 66, 42503 (2002).

[29] A. Derevianko, J. F. Babb, and A. Dalgarno, Phys. Rev. A 63, 052704 (2001).

[30] S. G. Porsev and A. Derevianko, J. Chem. Phys. 119, 844 (2003).

[31] W. T. Zemke and W. C. Stwalley, J. Chem. Phys. 114, 10811 (2001).

[32] C. Samuelis, E. Tiesinga, T. Laue, M. Elbs, H. Knöckel, and E. Tiemann. 63, 012710 (2000).

[33] O. Dulieu, P. S. Julienne, J. Chem. Phys. 103, 60 (1995).

[34] A. Grochola, W. Jastrzebski, P. Kowalczyk, and A. Pashov, J. Chem. Phys. 121, 5754 (2004).

[35] B. Bussery, Y. Achkar, M. Aubert-Frecon, Chem. Phys. 116, 319 (1987).

[36] P. Juncar, J. Pinar, J. Hamon and A. Chartier, Metrologia 17, 77 (1981).

[37] M. Tamanis, R. Ferber, A. Zaitsevskii, E.A. Pazyuk, A.V. Solyarov, Hongmin Chen, Jiangbing Qi, Henry Wang, W.C. Stwalley, J. Chem. Phys. 117, 7980 (2002).

[38] U. Diemer, H. Weickenmeier, M. Wahl, and W. Demtröder, Chem. Phys. Lett., 104, 489 (1984).

[39] S. B. Weiss, M. Bhattacharya and N. P. Bigelow, Phys. Rev. A 68, 042708 (2003).

Acknowledgments

First of all, I would like to thank a lot my supervisors Dr. Maris Tamanis and Prof. Ruvin Ferber for their guidance, help and support during all these years. I am extremely grateful to Dr. Asen Pashov, who taught me so many spectroscopy secrets, always gave a helping hand when I needed it and was not only a good colleague, but a real friend. Special thanks to Prof. Eberhard Tiemann, who kindly allowed to perform the experiments in his laboratory at the University of Hannover and fruitful discussions with whom opened me a lot of new knowledge in physics. I am also thankful to Dr. Horst Knöckel for his assistance and useful advices. My warmest thanks to Dr. Ilze Klincare for her friendly encouragement and help in physics and in life. I am also grateful to my colleagues Dr. Olga Nikolajeva and Jelena Zaharova for their friendly support. I would like to express also my gratitude to Dr. Andrey Stolyarov and Dr. Elena Pazyuk for sharing their valuable knowledge in molecular physics. I thank my family and friends for their love and understanding.

I acknowledge the support from the University of Latvia, Latvian Science Council, Morberg scholarship and European Social Fund.